Acta Geodyn. Geomater., Vol. 18, No. 4 (204), 511–524, 2021
DOI: 10.13168/AGG.2021.0037

journal homepage: https://www.irsm.cas.cz/acta

ORIGINAL PAPER

ARTEFACTS IN GRAVITY FIELD MODELLING

Jaroslav KLOKOČNÍK [1], Jan KOSTELECKÝ [2,3], Aleš BEZDĚK [1,4] * and Gunther KLETETSCHKA [5,6]

[1] *Astronomical Institute, Czech Academy of Sciences, CZ 251 65 Ondřejov, Fričova 298, Czech Republic*
[2] *Research Institute of Geodesy, Topography and Cartography, CZ 250 66 Zdiby 98, Czech Republic*
[3] *Faculty of Mining and Geology, VSB-TU Ostrava, CZ 708 33 Ostrava, Czech Republic*
[4] *Faculty of Civil Engineering, Czech Technical University in Prague, CZ 166 29 Praha 6, Czech Republic*
[5] *Department of Applied Geophysics, Charles University, Albertov 6, Praha 2, Czech Republic*
[6] *Geophysical Institute, University of Alaska Fairbanks, 903 N Koyukuk Drive, Fairbanks, AK, US*

**Corresponding author's e-mail:* bezdek@asu.cas.cz

ARTICLE INFO

Article history:
Received 16 August 2021
Accepted 11 October 2021
Available online 29 October 2021

Keywords:
Artefacts: graining
Aliasing
Along-track stripes
Gravity aspects
Gravity field models
Topography models

ABSTRACT

Artefacts in applications of the global gravity field and topographic models based on satellite and terrestrial data of diverse kinds are studied. Various types of artefacts are presented and analysed with the aim to understand how the artefacts originated, how to reduce them (if feasible) and to avoid misinterpretations in geoscience. We work with the gravity aspects (gravity anomalies, the Marussi tensor of the second derivatives of disturbing potential, gravity invariants and their specific ratio, strike angles, and virtual deformations), and with surface or bedrock topography. Examples for the Earth, the Moon, and Mars are presented.

1. INTRODUCTION:

ARTEFACTS OWING TO IMPERFECTIONS IN THE GRAVITY FIELD MODELS AND TOPOGRAPHY

Artefact is any error in the perception or representation of any information, introduced by the involved equipment or technique(s). The artefacts (ghosts, phantoms, chimerae, graining, strange shapes, wobbles, imps, gremlins, pitfalls, glitches …) are introduced by imperfect data, by a technology experimental error, by data processing, computational procedures or image processing or by combining data of various kinds, when some algorithms do something with data. It is a "man-made" entity.

Everybody who worked with any type of data has probably met a form of artefacts and a degradation of signal. We show examples mostly from the gravity field modelling, a branch of geodesy and geophysics. It means that we work with diverse satellite data (more in Sect. 2), terrestrial data (gravity anomalies) and surface or subglacial topography data (gathered by satellites). Besides this, we use also magnetic intensities (but not here) to support our results (interpretations) achieved with the gravitational/topography data.

The artefacts we present may serve as illustrative examples and may be taken as a warning to avoid misinterpretations and as a guide to remove the artefacts. We are not specialists on *pattern recognition,* a discipline dealing with the artefacts (see, e.g., Gonzales and Woods, 2002; Bishop, 2006), and have no ambitions to be.

We work with signals generated near the surface (~100 m) and locally modified by topography, with the gravity aspects derived from the global gravity field models of the Earth, the Moon and Mars. To us, the term "imperfect data" is related to its space and time resolution and distribution – irregular or insufficient, non-systematic coverage of the studied area, its precision/accuracy, resolvability, regularity, etc. The artefacts appear because we ask for "too much" (about results, products) from "too less" (about the input data).

We will demonstrate various types of artefacts:

(i) *Graining* of the signal when increasing the resolution of the computed parameter from the data set of not sufficient quality. The graining is increasing with increasing demands leading to a total disintegration, break-up, dispersion of the signal. The graining can be understood as an indicator of a forthcoming failure in the "high resolution" result. The artefact is defined by graining and that a failure of a presenting the calculations. For example, there is a spherical harmonic expansion of quantity V to certain

Cite this article as: Klokočník J, Kostelecký J, Bezděk A, Kletetschka G: Artefacts in gravity field modelling. Acta Geodyn. Geomater., 18, No. 4 (204), 511–524, 2021. DOI: 10.13168/AGG.2021.0036

maximum degree and order (d/o), but beyond certain d/o the calculation solutions start diverging and the artefacts will appear.

(ii) *Phantoming* - odd, bizarre, fantastic, looking, for example, like long walls of various forms, pyramids, circles and other ghosts, partly due to lack of data, partly from processing procedures and software.

(iii) *Data gapping* (for example, regions with missing bedrock topography, regions with data from ice penetrating radars in Antarctica) may yield false smoothed signal, expressing featureless areas.

(iv) *Aliasing* appears when we attempt reconstructing the original waveform from its samples and we have not sufficient amount of such samples. Aliasing represents a long-wave artefact due to not sufficient sampling in frequency space (insufficient data density); the shorter frequencies can have real context but hidden due to aliasing. Aliasing produces features like barriers, bulwarks, mounds, valleys, lakes, pyramid-like objects.

(v) *Striping*, organized along-track of satellite orbit bearing the instrument providing the data. They originate due to the irregular satellite altitude, different instrument condition (night vs. day radiation exposure conditions, solar wind activity) data coverage and gaps. When we compare density of the data along-track to that cross-track orbital components, we see remarkable differences between these two: one is high, one is low. In the case of specialised, nearly polar geodetic satellites used for gravity field studies, the along-track component is roughly in SN/NS direction while the cross-track goes along longitudes WE/EW.

A formal filtering of artefacts is possible using another way of plotting (image processing) or by a reduction of data resolution to sufficient level, or by employing of empirical mathematical filters (low pass or anti-aliasing filters to the input signal, by reconstruction filtering), e.g. Bentel et al. (2013). The final goal of working with artefacts from the computed entities is their realistic explanation and their subsequent reduction. We employ an actual "physical filtering", not a "mathematical masking". The actual progress is possible only with better data, their better space and time distribution, higher regularity in their distribution, better data coverage and control, incorporation of other data types or by implementation of realistic models helping to compute the required physical quantities.

First of all, we determine, how the artefacts originate and how they may look like in various situations. They are misleading for data interpretations. The examples of the artefacts for the Earth, the Moon and the Mars are provided in the main text (Sect. 4 for graining, Sect. 5 for bizarre shapes and data gaps, Sect. 6 for aliasing, and Sect. 7 for the along-track stripes) as well as in *Supplementary material* (http://www.asu.cas.cz/~jklokocn/Artefacts_2021_supplement/).

This work is based partly on our previous results (Klokočník et al., 2017 a, b, 2018, 2019, 2020 a-c, 2021). Here we put together our examples of artefacts in one "review".

2. METHOD AND DATA

We outline our theory, method and the data used in our analyses. We make use of the *gravity aspects (descriptors);* they are derived from the global static gravity field models of the Earth, the Moon, Mars or Venus. These are sets of spherical harmonic geopotential coefficients, known also as Stokes parameters, in the spherical harmonic expansions of the disturbing potential, well-known from geodesy and geophysics (see textbooks). We use the best data now available (see below).

2.1. NOTE ON THE METHOD

For the details of the theory about the gravity aspects see Klokočník et al. (2020a) with many references to other works. We work with the anomalies Δg (here with the gravity disturbances in spherical approximation), with the Marussi tensor of the second derivatives of the disturbing geopotential T_{ij}, namely with its radial component T_{zz}, with the gravity aspects I_1 and I_2 and their specific ratio I (a 2D indicator of the causative body), with the virtual deformations *vd* (they provide an alternative and concise representation of the Marussi tensor), and, in specific cases, with more or less one-way oriented ("combed") vectors of the strike angles θ. The strike angles θ are, in general, oriented chaotically; they can be in the given area aligned into one direction at the studied structure or form a halo around the impact craters. We have found the first practical application of the strike angles in Beiki and Pedersen (2010) for the impact crater Vredefort in Africa.

We put together the functions Δg, T_{ij}, I_1, I_2, I, and θ of the disturbing potential known from geophysics, we have defined and added *vd* (Kalvoda et al., 2013) and suggested a comprehensive name for all of them – *gravity aspects*. All these aspects are treated together to provide the most representative signature of the gravity sources (originating from density variations due to the causative bodies). We receive more information about the causative bodies with these aspects compared to the traditional Δg only. The gravity information is (where feasible) amended by topographic and other data. Via the gravity aspects we can detect subglacial volcanoes or lakes, trenches, surface and ground water, oil & gas localities (e.g., Klokočník and Kostelecký, 2015; Klokočník et al., 2020a) or paleolakes in Sahara (Klokočník et al., 2018, 2020b). Eppelbaum et al. (2017) studied tectonics also by means of virtual deformations.

The spatial distribution of the aligned strike angles becomes a new and accessible empirical geophysical tool for the recognition of potential oil&

gas or ground water deposits (Klokočník et al., 2021), paleolakes on the Earth (Klokočník et al., 2017, 2019, 2020c).

2.2. NOTE ON DATA

For the Earth, we used an excellent gravity filed model EIGEN 6C4 (Foerste et al., 2014; *E*uropean *I*mproved *G*ravity model of the *E*arth by *N*ew techniques), complete to maximum degree and order d/o = 2190, with the ground resolution 9 km and precision usually better than 10 mGal (depending on locality). The source of data was the space gradiometry from GOCE (*G*ravity field and steady-state *O*cean *C*irculation *E*xplorer, ESA). EIGEN 6C4 has improved terrestrial data base in comparison with its predecessor EGM 2008 (Pavlis et al., 2008 a, b, 2012), still without the GOCE data. In both these cases, terrestrial data came from NGA (National Geospatial-Intelligence Agency, USA), implemented by altimetry and additional data for EIGEN 6C4 (see Foerste et al., 2014 and GFZ Potsdam web pages).

We tested new gravity field models from GFZ, namely XGM2019e (Zingerle et al., 2020), EIGEN-6C4.2000.2100.exp.3660.gfc, shortly EIGEN-3660 and GOCE_DIR6.220.250.exp.-3660.gfc, shortly GOCE-DIR6 (Ince et al., 2020).

The XGM uses a terrestrial gridded dataset (up to d/o 720) provided by NGA. It should be an improved version of the terrestrial dataset used within EGM 2008. Above d/o 720, XGM uses over land topographic information, though, topography plays a minor role in this large desert, flat region.

EIGEN-3660 is EIGEN-6C4 that was augmented with the topographic model from d/o=2000 to d/o=3660. This model shall not be used for regions like Antarctica where EGM 2008 has gaps in the terrestrial data. GOCE-DIR6 was augmented with the topographic model from 200 to 3660. This gravity model concerns Antarctica. The ground resolution for d/o=3660 is about 4 km. We tested both these models together with the XGM (below), but continue to work with EIGEN 6C4.

For the Moon, we have among others (e.g. GRGM1200A, Lemoine et al., 2014), went up to d/o=1200, but used only d/o= 600 (recommended by the authors of the model). The reason for this recommendation is that the Kaula type power law constraint was applied to the harmonic coefficients for d/o >600 to stabilize the adjustment of harmonic geopotential coefficients.

The extensive truncation error tests (TET) with various limits d/o and for all our gravity aspects lead us to use the limit d/o=600, to avoid artefacts. GRGM1200A to 600 yields the ground resolution about 10 km and its precision 10 mGal.

For Mars, we employed NASA JPL JGMRO_120 F gravity model (Konopliv et al., 2020); the TET resulted here in a choice of the limit max d/o = 80. The relevant ground resolution is about 130 km.

Surface topography for the Earth is known from several models combining satellite, air-borne and terrestrial data. We use ETOPO1 DEM; it is a 1 arc-minute global relief model of Earth's surface that integrates land topography and ocean bathymetry (Amante and Eakins, 2009). ETOPO1 has a formal precision 10 m in height but when tested against ASTER GDEM and other models, in specific reasons, like Sahara, the height differences can be several times bigger.

The surface topography data about the Moon are taken from a new lunar digital elevation model from measurements of the LOLA (Lunar Orbiter Laser Altimeter), an instrument on the payload of Lunar Reconnaissance Orbiter spacecraft, and from SELENE Terrain Camera (Barker et al., 2016). The heights have nominal precision ~10 cm.

Mars topography comes from the MOLA on board of the MGS (Smith et al., 2001), achieving an accuracy of ~1 m radially and ~100 m in horizontal position. Given in resolution 0.25^0. The acronym *MOLA* means Mars Orbiter Laser Altimeter and *MGS* Mars Global Surveyor.

The standard bedrock topography for Antarctica is taken from the Bedmap 2 model (Fretwell et al., 2013); it contains among other quantities the bedrock elevation beneath the grounded ice sheet. It is given as a 1x1 km grid of heights of the bedrock above sea level; the actual spatial resolution is worse, 5x5 km or less. There are also large zones without any data (see Fretwell et al., 2013, pp. 379 and 388; the authors themselves call them “poles of ignorance” (PI, Fig. 4a).

A gravity-topography model SatGravRET2014 (Hirt et al., 2016), was the best available at the time of our analyses (searching for possible subglacial volcanoes, lakes, and impact craters, see Klokočník et al., 2017b and more). Its max d/o=2190, but is valid only for Antarctica. Roughly speaking SatGravRET2014 is a combination of recent satellite gravity data from GRACE and GOCE missions (close to EIGEN 6C4) with Bedmap2 and the Earth 2014 global topography model (Hirt et al., 2015). SatGravRET2014 increases the resolution of underlying gravity field models and decreases the resolution of Bedmap 2; the spatial resolution of SatGravRET2014 should be about 10 km over the whole Antarctica (excluding PIs and a close-pole zone), precision about 10 mGal.

We will present various artefacts found in physical quantities derived from the abovementioned models. This is not intended as a critique of these recent, still valid and quality models; it is a normal evolution to try to improve them. The existence of artefacts motivates for improvement of forthcoming data, procedures, and models derived.

3. A SIMPLE MODEL DESCRIBING THE ORIGIN OF ARTEFACTS

In the following demonstration “how the artefacts, concerning our work, may arise” we do not

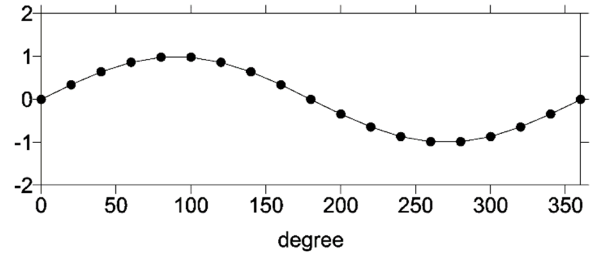

Fig. 1a Input data to Fourier analysis; data interval 20°.

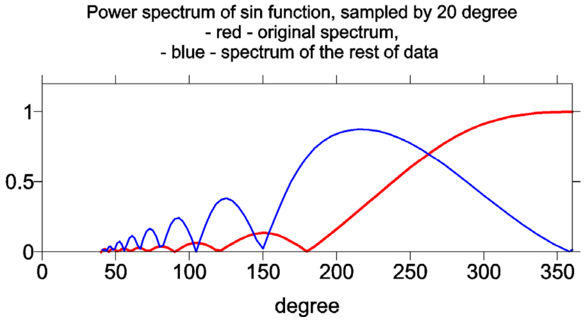

Fig. 1b Output from Fourier transform; the frequency spectrum with artefacts.

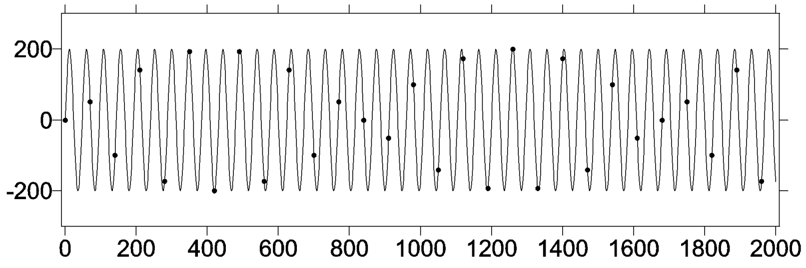

Fig. 1c The aliasing as a "long-wave" artefact, frequent and very well-known. The long wave is represented by the dots.

Table 1 The approximation of the "sine" in the interval <0°, 360°>. The most important frequencies, together with their amplitudes, after the Fourier transform of this sine function, with the gridded input data from Figure 1a.

Period [°]	**Amplitude**
360	1.0077
215	0.0131
150	0.0050

intend to explain the phenomenon "artefacts" in its entirety due to its broad occurrence (diverse specialisations) theory.

The input data (satellite as well as terrestrial) used to determine the static global gravity field models (= sets of harmonic geopotential coefficients) are gridded (not continuous), Figure 1a, and thus, the mathematical process from data to the coefficients may generate "false" harmonic frequencies. The process is a type of Fourier analysis (transform) [FT] from the data points given in specific data intervals (irregular in general) providing the coefficients.

Two types of artefacts appear: (a) a relatively long wave with shorter pseudowaves, Figure 1b. The long wave is real, the other waves are the artefacts, ghosts from the transform, and/or (b) a long wave, not real, together with a composition (aliasing) of waves shorter than the given data interval, Figure 1c, originating when only a few observations is available within the interval <0°, 360°>; in other words: suspicious and unrealistic wave may appear because the harmonic frequency cannot be discriminated. We offer a simple 1D approximation to reality (extended from Klokočník et al., 2019).

As an example, let us take the function "sine" on the interval <0°, 360°> defined by the individual data points given in an interval 20°, Figure 1a. In reality, this sampling interval is not known and can be irregular. After performing the FT, we receive a frequency spectrum (see Fig. 1b). Due to the gridding, we observe many frequencies, a "frequency fan", and not only the expected, "theoretical" period of 360°. The important frequencies and amplitudes generated by FT are summarized in Table 1.

If a process, containing a mixture of various periods, contains a hidden period

$$P_s \cong V,$$

where V is the sampling period, the value of the concealed periodic event will be equal to its initial value after certain number N of sampling periods. This occurs after $N \pm 1$ periods P_s (for $P_s < V < P_s$). Since the values are recorded only at discrete points at intervals V (sampling intervals), the periods V and P_s cannot be distinguished from one another but, roughly only after interval $N.V$. They will be manifest as one cycle of a longer pseudoperiod P_p. It holds approximately that $N.V \cong (N \pm 1).P_s$, $N.V \cong P_p$, and these two expressions then yield the pseudoperiod (aliasing wave)

$$P_p \cong P_s V / |V - P_s|$$

or vice versa: for the length of two concealed periods P_s which may generate a particular pseudoperiod P_p at a given sampling interval V

$$P_s \cong \frac{P_p V}{(P_p \pm \mathrm{V})} \cong V\left[1 \pm \left(\mathrm{V}/P_p\right)\right].$$

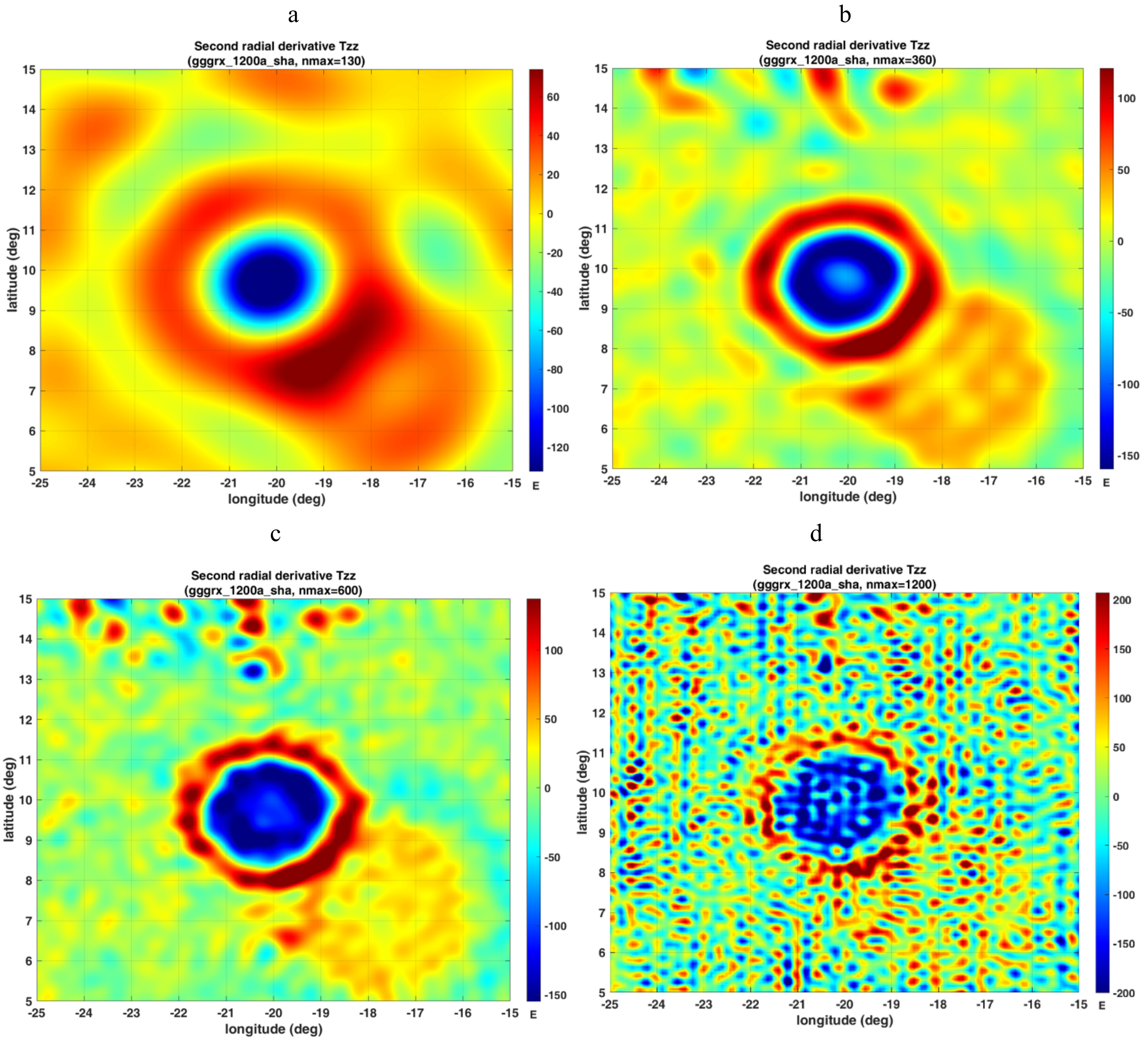

Figs. 2a-d Show T_{zz} [E] for the Moon's craters Copernicus and Copernicus H, computed from GRGM1200A, with maximum d/o limits 130, 360, 600, and 1200. The case (d) shows a total destruction (failure) of the gravity signal, when 1200 was used. Still worse and faster collapse was observed for the invariants.

The artefacts depend on density of the input data and on numerical precision of the transform. They can lead to misleading interpretations, it should be avoided. The example – utilizing Figures 1a and c – follows in Sect. 4.3.

4. ARTEFACTS

4.1. GRAINING

A graining (texture) of the signal appears when we ask for too much details in a physical quantity computed from specific data D which are not inherent to the data set D processed. For example, in the gravity field models developed to a certain maximum d/o, the authors of the model must use the Kaula rule for stabilization of the adjustment for the sought-for harmonic coefficients. Then the real data are replaced by a model, and the relevant part of the model, from the certain d/o to the maximum published d/o, should not be used. If we use it, the signal showing the gravity aspect starts to grain. The graining is increasing with increasing max d/o used, is more and more disturbing the underlying physical signal, up to its degeneration or a total failure.

Our examples here (and more in *Supplementary material*) present the cases of gravity field models for the Moon and Mars. Figures 2a-d show T_{zz} for the Moon's craters Copernicus and Copernicus H, computed from GRGM1200A, with d/o limits 130, 360, 600, and 1200. One loses information (details about T_{zz}) for the lowest d/o limit (Figs. 2 a, b). The graining starts at 600 (Fig. 2b) and is not acceptable for higher d/o limits ending with a total collapse of the gravity signal at d/o=1200 (Fig. 2d).

For Mars, Figures 3a-c show T_{zz} in a global view for d/o = 80, 100, and 120. The recommended limit d/o=80 (see Sect. 3) yields a reasonable choice;

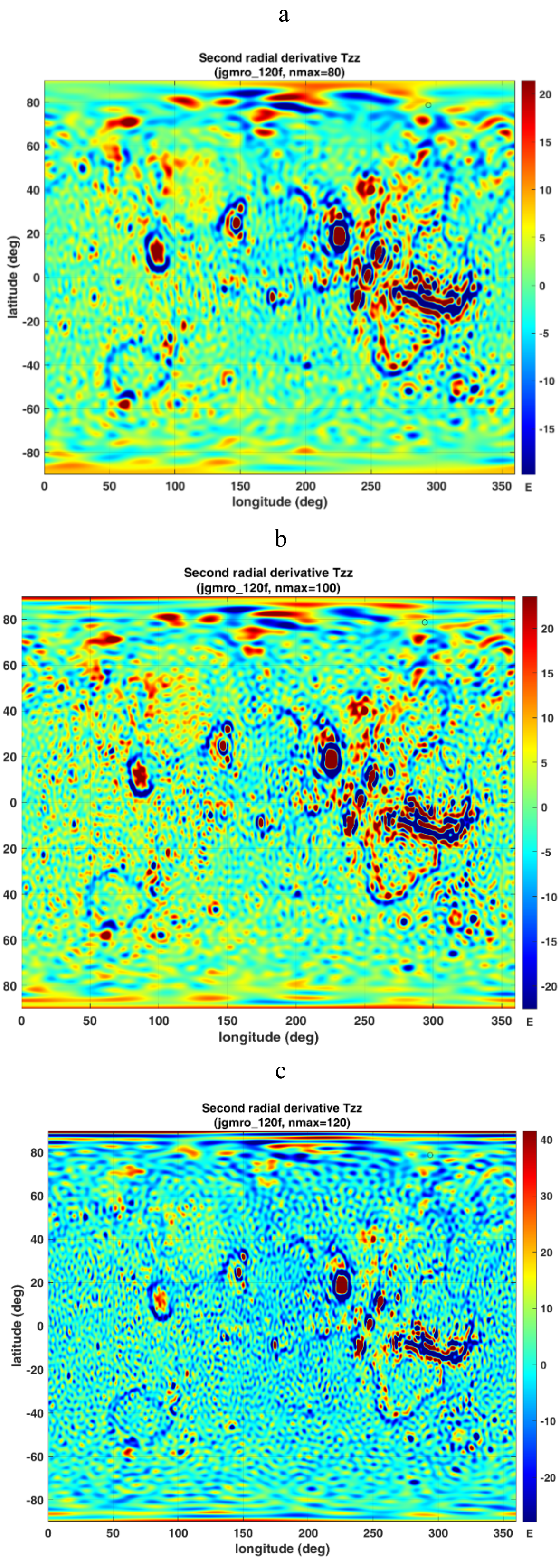

Figs. 3a-c A global look on T_{zz} [E] for Mars with GRGM1200A to d/o limits 80, 100, and 120.

computations to higher limits lead to evident signal degradation.

More examples in Supplementary material suggest that the degradation of the signal is faster for the higher derivatives of the disturbing potential, like the invariants, than for gravity disturbances.

4.2. BIZARRE SHAPES AND DATA GAPS

The bedrock topography model Bedmap 2 (Fretwell et al., 2013) is not based on a regular coverage of Antarctica by measurements, as we know from Sect. 2. The published network of altitudes and coordinates having step $1x1^0$ in a rectangular system lacks often the actual measurements. Then, the artefacts should be expected - when we will use the network literally as "$1x1^0$". Figure 4a shows the Gamburtsev Subglacial Mountains in East Antarctica partly well covered by dense data network, partly by tracks with data in distance about 50 km. In such a case the belts in between the tracks look smoothed. The tracks with data are clearly recognizable. One has therefore to be very careful to interpret results based on Bedmap2. In Figure 4a, we can see also two of PI zones (for example right hand side with large plain terrain – evident artefact). The zoom of Figure 4a is in Figure 4b and shows long narrow walls, sometimes straight, sometimes curved. Supplementary material shows additional ghosts: pyramid-like objects.

The user cannot do too much in this situation, only to decrease resolution; pursuit for too many details resulted in artefacts that will survive till the time when better data will become available. Analogical situation will be discussed in the case of satellite along-tracks stripes in Sect. 7. Here we distinguish the airplane tracks and different density of measurements along and cross-track. For along-track stripes, it will deal with different density of satellite measurements along-track and cross-track.

4.3. ALIASING

Figures 5 a-c (in the main text and more figures in Supplementary material) exhibit really peculiar "objects" in Sahara discovered when we computed the gravity aspects (in this example we present T_{zz}) with the EIGEN 6C4 to d/o/=2190 (and with the older model EGM 2008).

In the plain desert of Tunisia and Algeria, there was Chotts Megalake (now salt pans-sabkhas and a series of low-altitude saline seasonal lakes, marshland and basins) fed by several rivers from the Atlas Mountains and large river systems flowing from south from the central Sahara. Figure 5a shows our observation: strange, huge, rectangularly organized, linear structures looking like "walls" or "barriers" more than 100 km long, with a pyramid-like object inside the walls (positive Δg, T_{zz}), together with small size "graining" in large areas around (negative Δg, T_{zz}). It hardly can be a real (man-made) object (too extensive); see below. Also note circular structures in that area, mostly also with negative Δg and T_{zz}. Recall that sand surface in that area is generally flat, no big

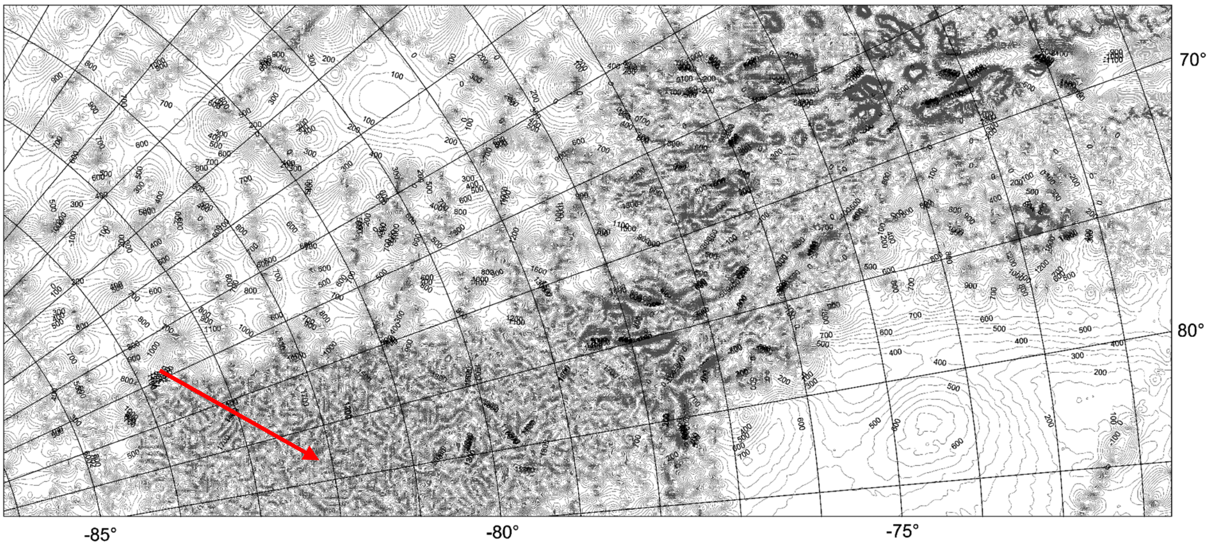

Fig. 4a Bedmap2 bedrock topography (Fretwell et al., 2013) in the Gamburtsev Subglacial Mountains in East Antarctica; denser data network in its central part, a lower density outside. Heights in metres above present-day sea level [m]. The topography data is published in 1x1^0 rectangular network. The actual data density is, however, lower; in the cross-track direction the airplane flight paths have about 7 km inside the Gamburtsev Subglacial Mountains and 50 km outside, but much better (more detailed) resolution along the flight tracks. When the stated density 1 degree is accepted literally and plotted in network 1x1^0, clearly we see many artefacts. We can detect dense vs. sparse airplane ground tracks along and across the airplane flights with dense (frequent) vs. scarce measurements, respectively, and two PI zones (zones without any data, upper left, bottom right). The north is to the right. The arrow shows one artefact of bizarre U shape (⊃). It is in Figure 4b in detail.

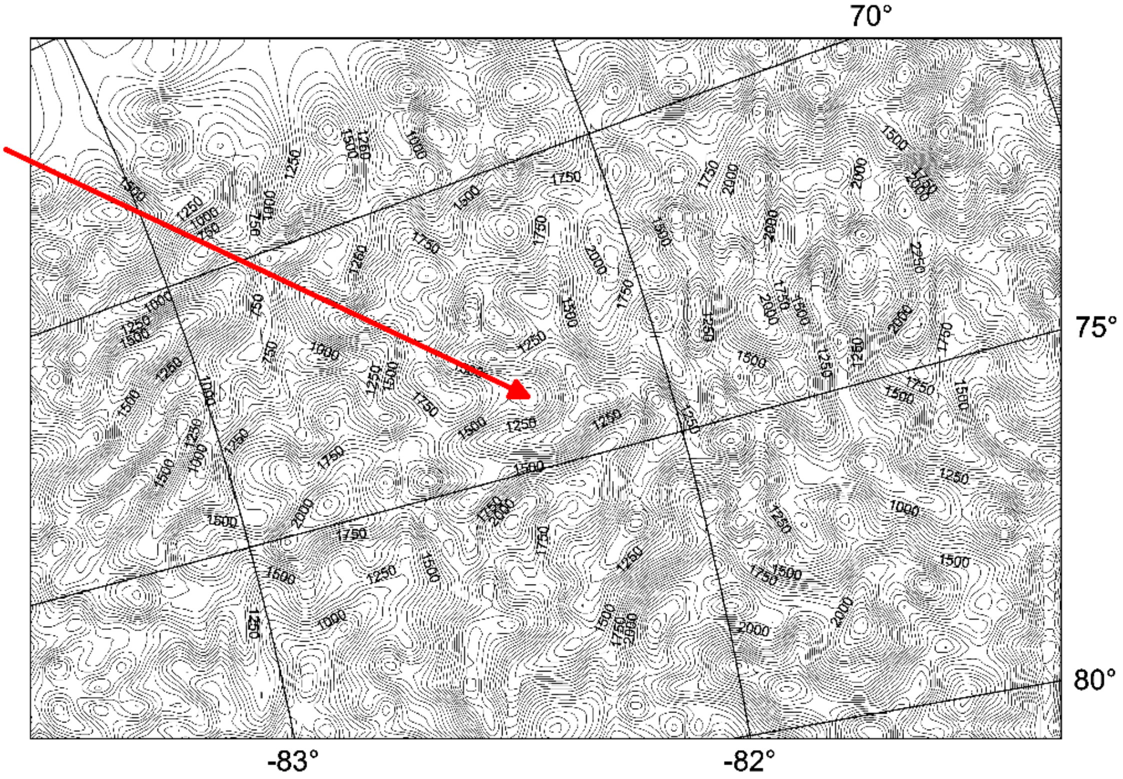

Fig. 4b The Bedmap 2 topography in the Gamburtsev Subglacial Mountains; example of artefacts; zoom and the arrow from Figure 4a.

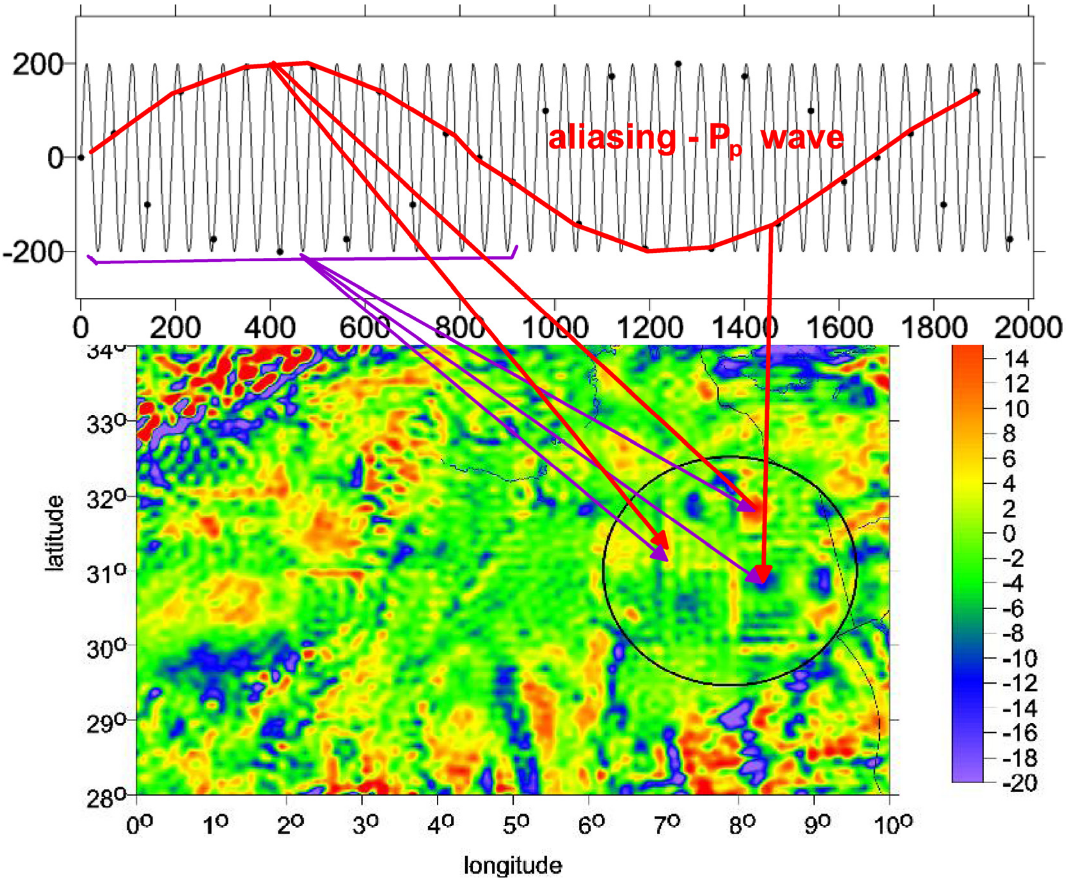

Fig. 5a The values of T_{zz} [E] from EIGEN 6C4 (to d/o=2190) in Sahara - Tunisia and Algeria, the Chotts paleo-megalake. The peculiar artefacts in desert (encircled) and graining are discussed in the text. Composition with Figure 1c. The aliasing P_p wave correlates fairly with artefact features shown by T_{zz} (see theoretical notes in Sect. 3 and text in this section). We use the relationship between the theory and a practical example in this case by means of the arrows relating P_p with T_{zz} (red for long waves, blue for short waves).

mountains south of Atlas - see ETOPO 1 topography in Supplementary material and ETOPO 1 together with T_{zz} here in Figure 5b.

The red arrows in Figure 5a are directed to the artefacts in T_{zz}; visible but not real. The blue arrows show real but hidden waves (see the brace in blue colour at the upper part of Fig. 5a); they have periods shorter than the sampling interval.

Strange thing is that these artefacts appear solely in this area of Sahara (we tested the whole Sahara). The quality of the terrestrial data from the US NGA database used in EGM 2008 and EIGEN 6C4 should be similar at all Sahara (this may be a false assumption; we have no information about the NGA gravity anomalies).

Our experience from the Great Sand Sea in west Egypt (Klokočník et al., 2017) is that the surface topography does not correlate with the gravity, because the former lacustrine and fluvial relief is buried under a thick layer of aeolian sands. It means that the traditional filling of missing gravity information by the topography does not take place here (for the tested gravity field models). We infer this from Figure 5 b.

We also tested the older EGM 2008 (2190) with similar database for terrestrial data as in EIGEN 6C4 and obtained the same artefacts at these locations (not shown here).

We decreased resolution of EIGEN 6C4 twice and the artefacts from Figure 5a nearly disappeared from the relevant plot. But this type of "filtering" is not preferred.

We also tested the new gravity field models from GFZ, labelled as XGM2019e (Zingerle et al., 2020), GOCE-3660, and EIGEN-2020 (Ince et al., 2020), see Sect. 3. With XGM, where dominant part over d/o=720 is eliminated, the artefacts are nearly gone. With EIGEN-2020 complete even up to d/o=3660, we can see similar results as with EIGEN6C4, with fine graining nearly everywhere and artefacts lines also west of the encircled zone (Fig. 5c).

We observe two types of artefacts in Figures 5 a-c (having the same reason): graining (already discussed above) and the phantoming (pyramids and walls). The origin of graining is in the use of too high d/o for the area with non-adequate data quality (a lower resolution). The aliasing is due mainly to under-sampling.

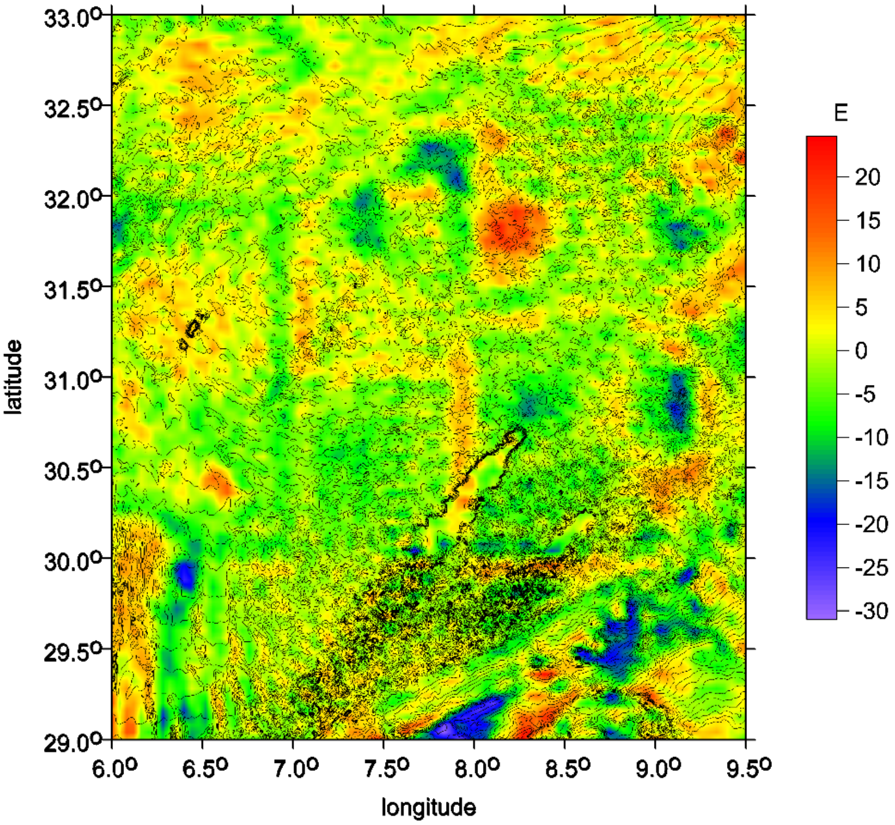

Fig. 5b A zoom from Figure 5a; the values of T_{zz} [E] from EIGEN 6C4 (to d/o=2190) with artefacts in T_{zz} plotted together with the surface topography from ETOPO 1 [m] in its maximum resolution.

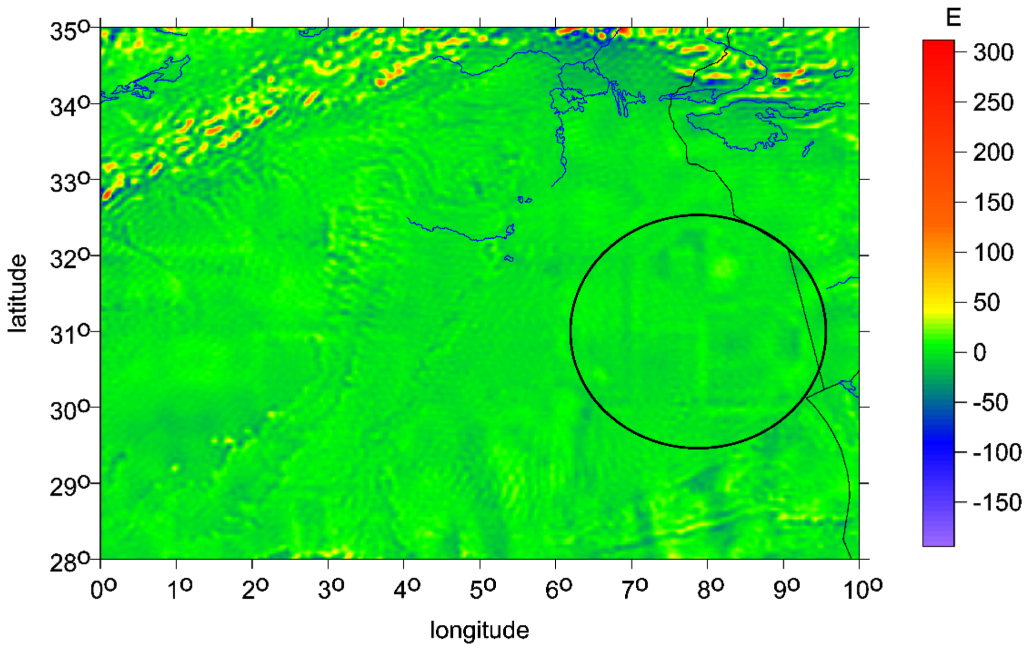

Fig. 5c The values of T_{zz} [E] from the EIGEN-2020 GFZ model (Ince et al., 2020) to d/o=3660; the same place as in Figure 5a, but intentionally with different scale. Note the peculiar artefacts in desert (circled) and fine graining, an indication that max. d/o used is too high and a symptom of forthcoming failure of the signal, nearly everywhere.

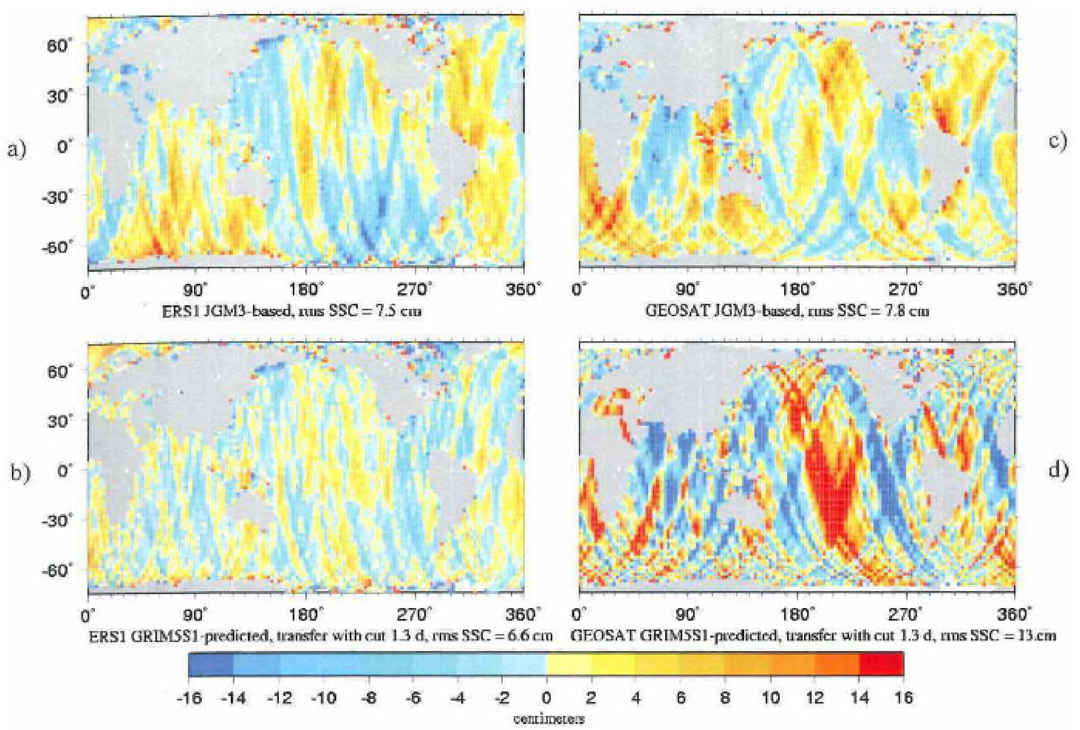

ERS1 JGM3-based, rms SSC = 7.5 cm
GEOSAT JGM3-based, rms SSC = 7.8 cm
ERS1 GRIM5S1-predicted, transfer with cut 1.3 d, rms SSC = 6.6 cm
GEOSAT GRIM5S1-predicted, transfer with cut 1.3 d, rms SSC = 13 cm

Fig. 6 Along-track stripes: typical situation for the two old altimetry satellites (ERS1 and Geosat) with two old gravity field models (JGM3 and GRIM5S1) – from around 1990-2000 [errors in cm]. Based on a GFZ report, serving later as a basis for Klokočník et al. (2002).

We deduce that these artefacts-phantoming originated due to problems in the terrestrial data base of NGA that infiltrated into all these gravity field models tested, to different models in different extent. Ordinary user has no detailed information available about the NGA terrestrial data. One knows nothing about possible data irregularities or about possible network for (airplane?) gravity anomalies measurements. Thus, he/she can do nothing, only to decrease resolution or use provisional mathematical filtering.

We don't rule out, although it is very improbable that the artefacts due to the aliasing (those long walls and "pyramids"), in some cases, are not artefacts, but real features. In the Great Sand Sea (west Egypt), the same kind of gravity aspects, predicted a paleolake/river system and possible settlements (but see Klokočník et al., 2017, 2020 a, b). It is obvious, however, that a "normal size" pyramids like those in Giza (all together) cannot produce the gravity signal of comparable magnitude. There are also tools how to estimate a probable depth of the relevant causative body; in the "Chotts case" in Figures 5a, b it would count several kilometres.

4.4. ALONG-TRACK STRIPES

Before satellite altimetry, the orbit precision had to consider data with their latitude and longitude that included both ascending and descending tracks. The altimetry required more detailed insight and the relevant theory has been worked out (Rosborough, 1986, who was the first; Rosborough and Tapley, 1987; and others). In those works, we observed how the radial orbit error of altimetry satellites or quality of experimental gravity field models based on fresh CHAMP observations and short arc orbits (Reigber et al., 2003, pp. 138, 263, 285…, $I = 87.3^0$, CHAllenging Minisatellite Payload) suffered from large variability, dependent of latitude and longitude.

It is now obvious that these patterns are artefacts that disappeared in newer "well mixed" and "correctly weighted" gravity field models (without dominance of the CHAMP data in the experimental models) from diverse data sources (various satellite as well as terrestrial data sets). An empirical filtering had no sense; just more data and realistic relative weights were needed to overcome this problem. We studied the radial orbit error by means of single and dual-satellite crossovers with the goal to minimize the former by the latter (e.g. Klokočník et al., 2002, 2005; Wagner et al., 1997).

Since that time, we can see that this type of artefacts appears again and again and the recommendation how to get rid of them is the same and evident: to achieve better data and meantime to reduce resolution of our products.

The origin of the along-track stripes is basically the same everywhere. One deals with irregular data density along-track and cross-track. For the polar orbits, frequently used in the gravity field research, it

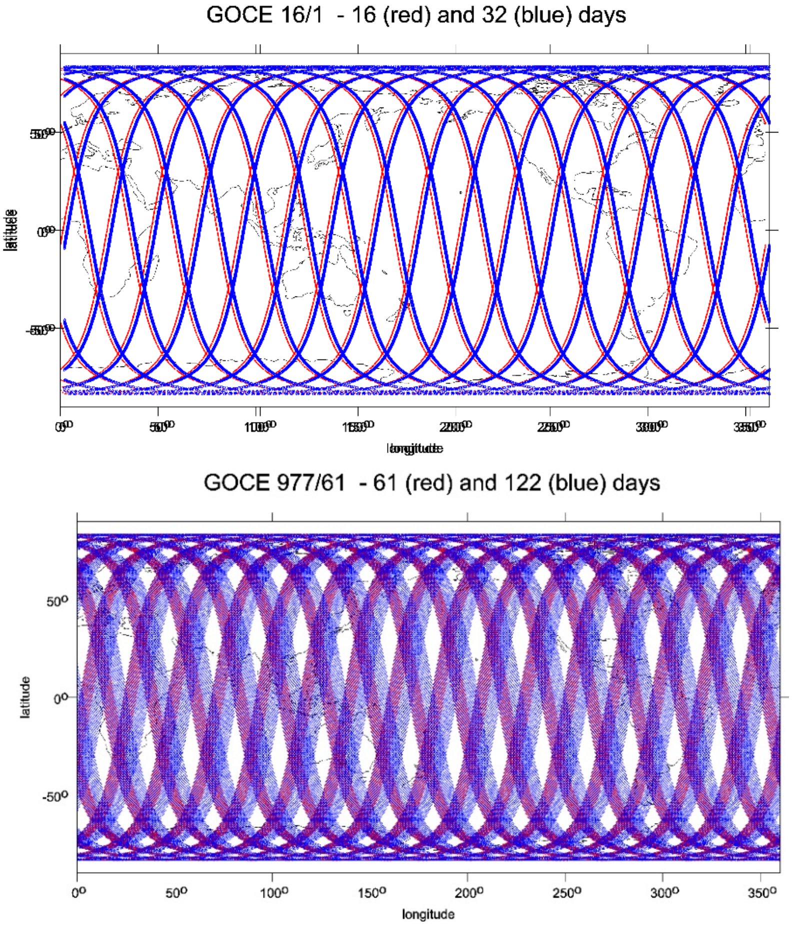

GOCE 16/1 - 16 (red) and 32 (blue) days

GOCE 977/61 - 61 (red) and 122 (blue) days

Figs. 7 a, b Ground tracks of nearly polar GOCE orbit at two different heights of flight (semimajor axis of satellite orbit) for two different orbital resonances *β/α* [rev/day] and various time intervals. Note the increasing global coverage with increasing *α* [days]. Note the gaps in longitude till the interval of "winding" of the ground tracks around the globe is not complete, i.e. *α* days.

means that measurements taken along the orbit in NS/SN, following direction of the ascending or descending orbital arcs, are frequent, say each second. It corresponds to ~8 km distance, while the ground-track distances in EW/WE (cross-track) are much higher, even hundred kilometres. This inevitably results in the troubles.

The goal is to reduce this imbalance, in other words, to achieve as similar as possible resolutions in both along and cross track directions. We can influence this situation by clever orbit selection, if we have a correction thruster on board – more about it below. The orbit selection will move the orbit to high order orbital resonance. Altimetry satellites and GOCE provide a good example of the orbit tuning – small change in semimajor axis leads to a big change of the repeat period. Now, it is useful to recall definition of orbital resonance.

The satellite is in orbit resonance *β/α* [rev/day] when it performs *β* [rev] nodal revolutions per *α* [day] sidereal days (*β*, *α* prime integers). Then, geometrically, after *α* days, the orbit repeats exactly with respect to the ground observers (we speak about repeat orbit *β/α* and repeat period *α*).

Orbital (and rotational) resonances are frequent in the solar system. For the Earths artificial satellites, they were utilized for gravitational studies, first to determine linear combinations of the harmonic geopotential coefficients of the resonant order $\beta\gamma$ ($\gamma=1,2\ldots$), then to assess the accuracy of the global gravity field models for selected orders $\beta\gamma$ and then for orbit choice of altimetry satellites or GOCE and planetary orbiters (Klokočník et al., 2010, 2013).

Figures 7 a,b show the ground tracks of nearly polar GOCE orbit at two different semimajor axes of and two resonances *β/α*. Note the increasing global coverage with increasing *α* [days] because the density of ground track in longitude is higher. The ground track distance in longitude at the equator for the 16/1 resonance would be $360{:}16=22.5^0$, equivalent to 2475 km. With gradiometer measurement density along-track each second, i.e. ~8 km, we have a large disproportion between latitudinal and longitudinal coverage/resolution, i.e. the reason for the along-track stripes for example in geoid undulations based on gravity field model derived from the data affected by that disproportionality. Thus, we seek, accounting for the type of experiment, for a free-falling orbit

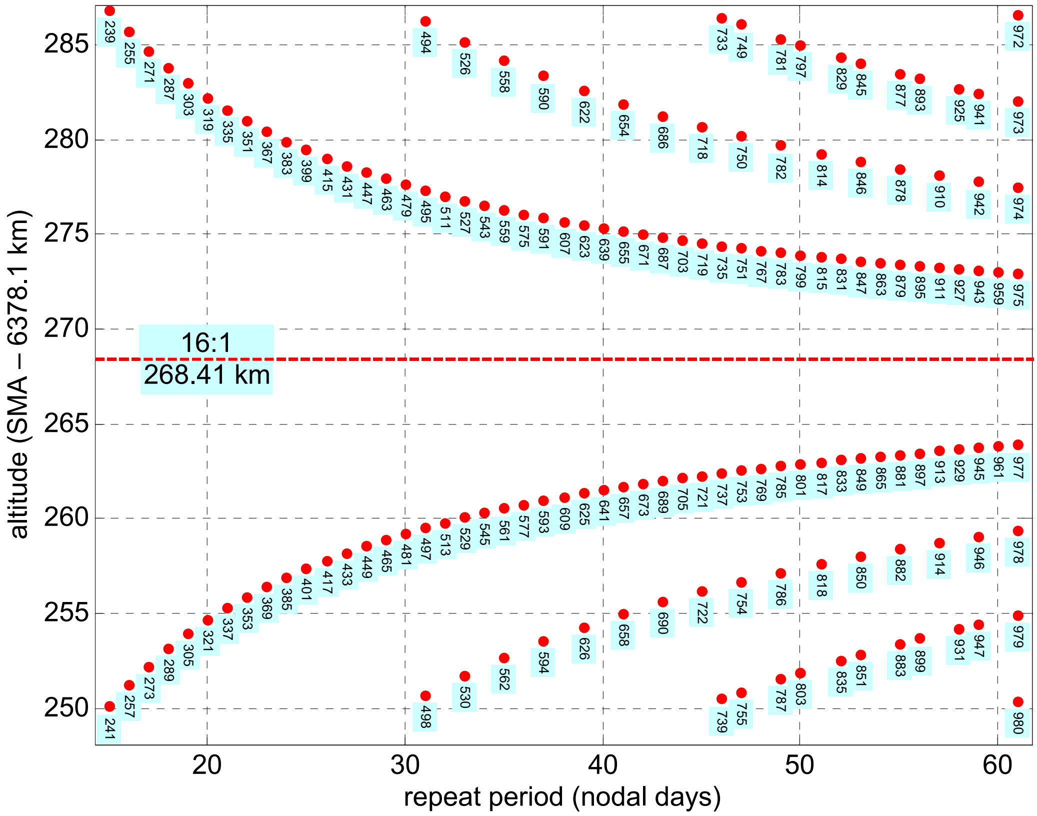

Fig. 8 Resonant diagram for GOCE *β/α* for specific orbital inclination (here $I = 96.7^0$ which means retrograde, nearly polar orbit). We have the repeat period *α* [day] on the x-axis and altitude (semimajor axis of satellite orbit minus reference radius of the planet) [km] on the y-axis. Dots show the relevant *β* [revolutions in degree]. Without orbit correcting manoeuvres, the orbit would decay slowly, decreasing the altitude, due to the atmospheric drag. With active correcting manoeuvres, the orbit can be kept at prescribed, required orbit, i.e. in the selected *β/α* resonance (with inaccuracy given by the motor ability)

(GRACE) or for a high resonant-orbit (kept at some high *β*) (GOCE). The higher *β*, the longer repeat period *α* (for specific narrow interval of semimajor axis) and more strict requirements on correct function of the ion engine on board of GOCE. Its nominal precision for orbit height keeping was 50 m, achieved accuracy was 5 m.

Earth's satellites orbital tuning (Klokočník et al., 2003, 2008, 2013) and planetary orbiters (Klokočník et al., 2010) would correct these data. Our proposal for GOCE orbit choice at the high resonance (61-day repeat orbit, *β/α* = 977/61) has resulted in the extended, final stage of GOCE work in space with remaining fuel (e.g., Bezděk et al., 2009, 2010).

How to do the orbit tuning with onboard ion engines? Resonant diagrams (e.g., Klokočník et al 2008, 2013) for GOCE for specific orbital inclination (here $I = 96.7^0$ which means retrograde, nearly polar orbit) is in Figure 8. We have the repeat period *α* on the x-axis and altitude (semimajor axis of satellite orbit minus reference radius of the planet) on the y-axis. Red dots show the relevant *β*. Without orbit correcting manoeuvres, the orbit would decay slowly, decreasing the altitude, due to the atmospheric drag (the case of GRACE for example, figures in Supplementary material). With active correcting manoeuvres, the orbit can be kept at the prescribed, preselected high resonant orbit to minimize the difference in ground coverage along and cross-track.

For example: with *β/α*=977/61*,* we have the cross-track ground distance at equator ~40 km (with *β/α*=16/, it was 2475 km).

5. CONCLUSION

Artefacts are everywhere where we work with data. Here we present examples, not theory, from our branch and for our branch. The artefacts can be misleading for interpretations and thus, our wish is to understand "how it works" and suppress or remove them if possible. This work is not intended as a critique of the gravity field and topography models used; it is a normal evolution to improve them. The artefacts, among others, motivate for improvements.

Various types of artefacts can be encountered during our gravity field studies and within the work with the surface/bedrock topography data concerning the Earth, the Moon or Mars during the last 20 years these data were presented and discussed. Our results should serve as paradigms, examples and warning to avoid misinterpretations of various products from gravity field models or topography data infected by the artefacts and as a guide what eventually one can do to reduce the artefacts.

Graining in the gravity aspects from the global gravity field models was documented on a case of the second radial derivative T_{zz} for the Moon's crater Copernicus (Figs. 2 a, b) and for a global view on Mars (Figs. 3a-c). The graining starts at d/o = 600 (Fig. 2b) and above d/o = 80 (Figs. 3a-c), respectively, in both cases at the limit where the Kaula rule started to be used to stabilize least squares adjustments for the harmonic geopotential coefficients of the respective gravity model. With increasing maximum d/o above these limits, the gravity signal (T_{zz} here) is more and more graining, till a final collapse (Fig. 2d, Fig. 3c and Supplementary material).

In conclusion for the graining: we asked "too much" from the data which did not contain "enough" information. The graining can be understood as a symptom of a forthcoming signal failure, which would appear at higher d/o, when we ignore a warning coming by increasing granulation (compare Figs. 2a-c to 2d; for more examples see Supplementary material).

Phantoming - odd, bizarre, fantastic features, has been documented on the case of Bedmap 2 bedrock topography for Antarctica (example in Fig. 4a). Bedmap 2 is a fantastic tool to study Antarctica. It is provided in a network 1×1^0, but still often with much sparser actual data than 1×1^0, sometimes with large data gaps (over hundred kilometres). These sparser data and gaps inevitably produce artefacts if we do not wish to decrease the resolution (one example is in Figure 4b, more in Supplementary material).

Another strange example is for the artefacts on Sahara (Fig. 5a); we found that the probable reason for them is hidden in the terrestrial data base common and used for the relevant gravity field model, for which we however have no detailed information (NGA).

In this case, the user cannot do too much, just to decrease resolution of his/her products, to avoid pseudo-optimistic interpretations, and wait for better data.

The *along-track striping* is due to irregular data coverage and gaps; when we compare density of the data along-track to that cross-track orbital components for nearly polar geodetic satellites like GOCE, we can see a remarkable difference between these two: one is high, one is low. We show examples mainly for the gravity mission GOCE with instructions how to tune the orbit of GOCE by onboard motors in altitude (Figs. 7a, b, 8; for more figures see Supplementary material, http://www.asu.cas.cz/~jklokocn/Artefacts_2021_supplement/) to get better orbital resonant regime partly avoiding the disproportion in those two directions.

ACKNOWLEDGMENTS

This work was prepared in the frame of projects RVO 67985815 (Czech Academy of Sciences) and LO1506 (PUNTIS) provided by the Ministry of Education, Youth and Sports of the Czech Republic. GK was partially supported from the Czech Science Foundation 20-08294S, ME, LTAUSA 19141. We thank Drs. P. Zingerle and Ch. Foerste from GFZ, Potsdam.

REFERENCES

Amante, C. and Eakins, B.W.: 2009, ETOPO1 1. Arc-Minute Global Relief Model: procedures, data sources and analysis. NOAA TM NESDIS NGDC-24. DOI: 10.7289/V5C8276M

Barker, M.K., Mazarico, E., Neumann, G.A., Zuber, M.T., Haruyama, J. and Smith, D.E.: 2016, A new lunar digital elevation model from the Lunar Orbiter Laser Altimeter and SELENE Terrain Camera. Icarus, 273, 346-355. DOI: 10.1016/j.icarus.2015.07.039

Beiki, M. and Pedersen, L. B.: 2010, Eigenvector analysis of gravity gradient tensor to locate geologic bodies. Geophysics, 75, 137-149. DOI: 10.1190/1.3484098

Bentel, K., Schmidt, M. and Denby, C.R.: 2013, Artifacts in regional gravity representations with spherical radial basis functions. J. Geod. Sci., 3, 173-187. DOI: 10.2478/jogs-2013-0029

Bezděk, A., Klokočník, J., Kostelecký, J., Floberghagen, R. and Gruber, C.: 2009, Simulation of free fall and resonances in the GOCE mission. J. Geod., 48, 1, 47–53. DOI: 10.1016/j.jog.2009.01.007

Bezděk, A., Klokočník, J., Kostelecký, J., Floberghagen, R. and Sebera, J.: 2010, Some aspects of the orbit selection for the measurement phases of GOCE. Proc. ESA Living Planet Symposium, Bergen, Norway, 28 June – 2 July, 2010, ESA SP-686.

Bezděk, A., Sebera, J., Klokočník, J. and Kostelecký, J.: 2014, Gravity field models from kinematic orbits of CHAMP, GRACE and GOCE satellites. Adv. Space Res., 53, 412–429. DOI: 10.1016/j.asr.2013.11.031

Bishop, Ch.M.: 2006, Pattern Recognition and Machine Learning. Information Sciences and Statistics. Springer-Verlag, New York.

Bucha, B. and Janák, J.: 2013, A MATLAB-based graphical user interface program for computing functionals of the geopotential up to ultrahigh degrees and orders. Comput. Geosci, 56, 186-196. DOI: 10.1016/j.cageo.2013.03.012

Eppelbaum, L.V. and Katz, Yu.I.: 2017, A new regard on the tectonic map of the Arabian-African region inferred from the satellite gravity analysis. Acta Geophys., 65, 607-626. DOI: 10.1007/s11600-017-0057-2

Fretwell, P., Pritchard, H., Vaughan, D., Bamber, J. et al.: 2013, Bedmap2: improved ice bed, surface and thickness datasets for Antarctica. Cryosphere, 7, 375–393. DOI: 10.5194/tc-7-375-2013

Gonzales, R.C. and Woods, R.: 2002, Digital image processing, 2/E. Prentice Hall, NJ07458, ISBN 0-20-118075-8.

Hirt, Ch. and Rexer, M.: 2015, Earth 2014: 1 arc-min shape, topography, bedrock and ice-sheet models—available as gridded data and degree-10,800 spherical harmonics. Int. J. Appl. Earth Obs. Geoinf., 39, 103–112. DOI: 10.1016/j.jag.2015.03.001

Hirt, Ch., Rexer, M., Scheinert, M., Pail, R., Claessens, S. and Holmes, S.: 2016, A new degree-2190 (10 km resolution) gravity field model for Antarctica developed from GRACE, GOCE and Bedmap 2 data. J. Geod., 90, 105–127. DOI: 10:1007/s00190-015-0857-6

Ince, E.S., Abrykosov, O., Förste, C. and Flechtner, F.: 2020, Forward gravity modelling to augment high-resolution combined gravity field models. Surv. Geophys., 41, 767-804. DOI: 10.1007/s10712-020-09590-9

Klokočník, J., Bezděk, A., Kostelecký, J. and Sebera, J.: 2010, Orbit tuning of planetary orbiters for accuracy gain in gravity-field mapping. J. Guid. Control Dyn., 33, 3, 853–861. DOI: 10.2514/1.46223

Klokočník, J., Gooding, R.H., Wagner, C.A., Kostelecký, J. and Bezděk, A.: 2013, The use of resonant orbits in satellite geodesy: A review. Surv. Geophys., 34, 43–72. DOI: 10.1007/s10712-012-9200-4

Klokočník, J., Kostelecký, J. and Bezděk, A.: 2017, Gravitational atlas of Antarctica. Springer Geophysics, 113 pp. DOI: 10.1007/978-3-319-56639-9

Klokočník J., Kostelecký, J. and Bezděk, A.: 2019, The putative Saginaw impact structure, Michigan, Lake Huron, in the light of gravity aspects derived. J. Great Lakes Res., 45, 1, 12-20. DOI: 10.1016/j.jglr.2018.11.013

Klokočník, J., Kostelecký, J., Bezděk, A. and Cílek, V.: 2021, The spatial distribution of the strike angles derived from EIGEN 6C4 gravity model - A new possibility for oil&gas exploration? Int. J. Oil, Gas and Coal Technology, 28, 3, 306–332. DOI: 10.1504/IJOGCT.2021.10037627

Klokočník, J., Kostelecký, J., Bezděk, A. and Kletetschka, G.: 2020c, Gravity strike angles: a modern approach and tool to estimate the direction of impactors of meteoritic craters. Planet. Space Sci., 194, 105113. DOI: 10.1016/j.pss.2020.105113

Klokočník, J., Kostelecký, J. and Cílek, V.: 2020a, Subglacial and underground structures detected from recent gravito-topography data. Cambridge Scholars Publishing, 252 pp.

Klokočník, J., Kostelecký, J., Cílek, V., Bezděk, A. and Pešek, I.: 2017, A support for the existence of paleolakes and paleorivers buried under Saharan sand by means of gravitational signal from EIGEN 6C4. Arab. J. Geosci., 10, 199. DOI: 10.1007/s12517-017-2962-8

Klokočník, J., Kostelecký, J., Cílek, V., Bezděk, A. and Pešek, A.: 2018, Gravito- topographic signal of the Lake Vostok area, Antarctica, with the most recent data. Polar Sci., 17, 59–74. DOI: 10.1016/j.polar.2018.05.002

Klokočník, J., Kostelecký, J. and Gooding, R.H.: 2003, On fine orbit selection for particular geodetic and oceanographic missions involving passage through resonances. J. Geod., 77, 30–40. DOI: 10.1007/s00190-002-0276-3

Klokočník, J., Kostelecký, J., Varadzinová, L, Bezděk, A. and Kletetschka, G.: 2020b, A gravity search for oil and gas and groundwater in Egypt using the strike angles derived from EIGEN 6C4. Appl. Sci., 10, 8950. DOI: 10.3390/app10248950

Klokočník, J., Kostelecký, J., Wagner, C.A., Schwintzer, P., Förste, Ch. and Scharroo, R.: 2005, Evaluation of the accuracy of the EIGEN-1S & 2 CHAMP-derived gravity field models. J. Geod., 78, 7-8, 405–417.

Klokočník, J., Reigber, CH., Schwintzer, P., Wagner, C.A. and Kostelecký, J.: 2002. Evaluation of pre-CHAMP gravity models `GRIM5-S1' and `GRIM5-C1' with satellite crossover altimetry. J. Geod., 76, 189–198. DOI: 10.1007/s00190-001-0240-7

Klokočník, J., Wagner, C.A, Kostelecký, J. and Bezděk, A.: 2015, Ground track density considerations on the resolvability of gravity field harmonics in a repeat orbit. Adv. Space Res., 56, 1146–1160. DOI: 10.1016/j.asr.2015.06.020

Klokočník, J., Wagner, C.A., Kostelecký, J. and Jandová, M.: 1995, The filtering effect of orbit correction on geopotential errors. J. Geod., 70, 146–157. DOI: 10.1007/BF00943690

Klokočník, J., Wagner, C.A., Kostelecký, J., Bezděk A., Novák, P. and McAdoo, D.: 2008, Variations in the accuracy of gravity recovery due to ground track variability: GRACE, CHAMP and GOCE. J. Geod., 82, 12, 917–927. DOI: 10.1007/s00190-008-0222-0

Pavlis, N.K., Holmes, S.A., Kenyon, S.C. and Factor, J.K.: 2008a, An Earth gravitational model to degree 2160: EGM2008. EGU General Assembly 2008, Vienna, Austria.

Pavlis, N.K., Holmes, S.A, Kenyon, S.C. and Factor, J.K.: 2008b, EGM2008: an overview of its development and evaluation. National Geospatial-Intelligence Agency, USA. Int. Conf. on Gravity, Geoid and Earth Observation 2008, Chania, Crete, Greece.

Pavlis, N.K., Holmes, S.A., Kenyon, S.C. and Factor, J.K.: 2012, The development and evaluation of the Earth gravitational model 2008 (EGM2008). J. Geophys. Res., 17, B04406. DOI: 10.1029/2011JB008916

Reigber, C., Balmino, G., Schwintzer, P. et al.: 2003, New global gravity field models from selected CHAMP data sets. In: Reigber, C., Lühr, H., Schwintzer, P. (eds), First CHAMP Mission Results for Gravity, Magnetic and Atmospheric Studies. Springer, Berlin, Heidelberg. DOI: 10.1007/978-3-540-38366-6_18

Rosborough, G.W.: 1986, Satellite orbit perturbations due to the geopotential. CSR-86-1 Rep., Center for Space Research, Univ. of Texas, Austin.

Rosborough, G.W. and Taply, B.D.: 1987, Radial, transverse and normal satellite position perturbations due to the geopotential. Celest. Mech., 40, 409-421. DOI: 10.1007/BF01235855

Smith, D.E., Zuber, M.T., Frey, H.V., Garvin, J.B., Head, J.W., Muhleman, D.O. et al.: 2001, Mars orbiter laser altimeter: Experiment summary after the first year of global mapping of Mars. J. Geophys. Res., 106, 23689–23722. DOI: 10.1029/2000JE001364

Wagner, C.A., Klokočník, J. and Kostelecký, J.: 1997, Dual-satellite crossover latitude-lumped coefficients, their use in geodesy and oceanography. J. Geod., 71, 603–616. DOI: 10.1007/s001900050128

Wagner, C.A., McAdoo, D., Klokočník, J. and Kostelecký, J.: 2006, Degradation of geopotential recovery from short repeat-cycle orbits: application to GRACE monthly fields. J. Geod., 80, 2, 94–103. DOI: 10.1007/s00190-006-0036-x

Zingerle, P., Pail, R., Gruber, T. and Oikonomidou, X.: 2019, The experimental gravity field model XGM2019e. GFZ Data Services. DOI: 10.5880/ICGEM.2019.007